Summary of the 2021 Asian Summer Monsoon

This report summarizes the characteristics of the surface climate and atmospheric/oceanographic considerations related to the Asian summer monsoon for 2021.

Note: The Japanese 55-year Reanalysis (JRA-55; Kobayashi et al. 2015) atmospheric circulation data and COBE-SST (Ishii et al. 2005) sea surface temperature (SST) data were used for this investigation. NOAA Interpolated Outgoing Longwave Radiation (OLR) data (Liebmann and Smith 1996) provided by the U.S. NOAA Earth System Research Laboratory (ESRL) from their web site at https://www.esrl.noaa.gov/psd/ was referenced to infer tropical convective activity. The base period for the normal is 1991 to 2020. The term "anomaly" as used in this report refers to deviation from the normal.

1. Precipitation and temperature

CLIMAT data on four-month total precipitation for the summer monsoon season (June – September) show more than 140% of the normal in central and northern East Asia, in Indonesia, and in/around southwestern Pakistan, while values less than 60% of the normal were seen in northwestern China and southwestern Central Asia (Figure 3-1 (a)). Monthly precipitation for August in western Japan was the highest on record since 1946. Heavy rain caused more than 300 fatalities in central China from mid- to late July (Chinese Government) and more than 1,000 fatalities in/around South Asia from June to August (governments of India/Pakistan/Nepal, European Commission).

Four-month mean temperatures for the same period were above normal in many parts of East and Central Asia, while values were below normal in northern East Asia and part of Southeast and South Asia (Figure 3-1 (b)). Monthly mean temperatures were the second highest for June and the third highest for July in northern Japan since 1946 (Japan Meteorological Agency) and the second highest for July in China since 1961 (China Meteorological Administration).

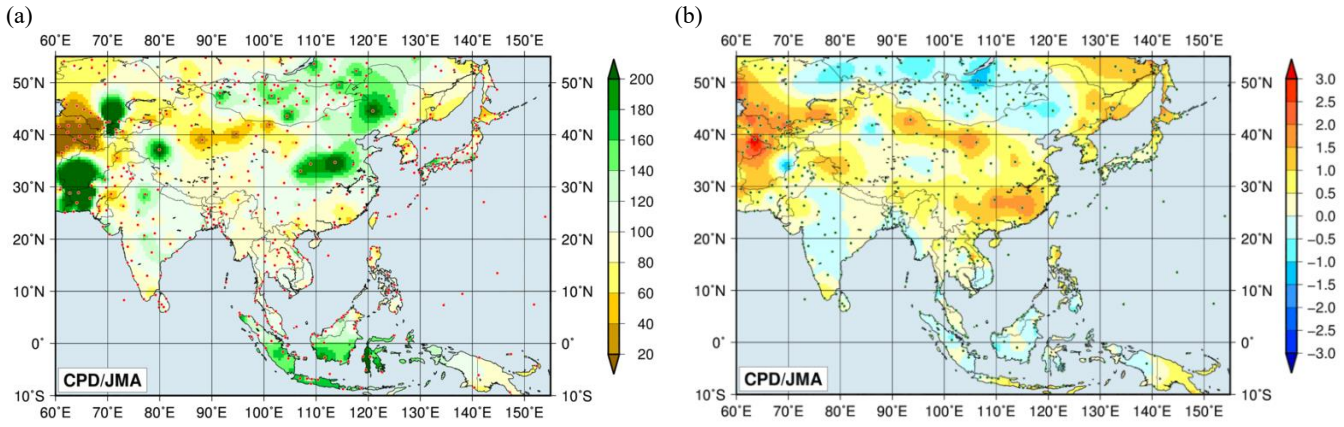

Figure 3-1 Four-month (a) precipitation ratios [%] and (b) mean temperature anomalies [°C] from June to September 2021
The base period for normal is 1991 – 2020. The red (a) and green (b) dots show stations providing map data, which are interpolated due to a lack of CLIMAT reporting and climatological normal values in some areas.

2. Tropical cyclones

A total of 16 named tropical cyclones (TCs) had formed over the western North Pacific and the South China Sea by September 2021, as compared to the normal of 18.6 (Table 3-1). From June to September, a total of 13 named TCs (climatological normal: 16.1) formed, with 10 approaching or making landfall on East Asia and 8 (climatological normal: 9.5) approaching or making landfall on Japan.

In late July, Typhoon In-Fa passed over Japan's Okinawa region with a maximum wind speed of 85 knots and made landfall on eastern China, bringing rainfall of 283.5 mm from 21st to 24th July in Naha, Japan (monthly climatological normal for July: 188.1 mm) and more than 170 mm from 24th to 27th July in Shanghai, China (monthly climatological normal for July: 144.1 mm).

Table 3-1 Tropical cyclones reaching TS intensity or higher formed over the western North Pacific and the South China Sea by September 2021

Name (number)		Date (UTC)	Category[1)]	Maximum wind[2)] (kt)
Dujuan	(2101)	18 Feb - 21 Feb	TS	40
Surigae	(2102)	13 Apr - 24 Apr	TY	120
Choi-wan	(2103)	30 May - 5 Jun	TS	40
Koguma	(2104)	11 Jun - 13 Jun	TS	35
Champi	(2105)	23 Jun - 27 Jun	TY	65
In-fa	(2106)	17 Jul - 27 Jul	TY	85
Cempaka	(2107)	18 Jul - 21 Jul	TY	70
Nepartak	(2108)	23 Jul - 28 Jul	TS	40
Lupit	(2109)	4 Aug - 8 Aug	TS	45
Mirinae	(2110)	5 Aug - 9 Aug	STS	50
Nida	(2111)	4 Aug - 7 Aug	STS	55
Omais	(2112)	20 Aug - 23 Aug	TS	45
Conson [3)]	(2113)	6 Sep - 11 Sep	STS	55
Chanthu [3)]	(2114)	7 Sep - 18 Sep	TY	115
Dianmu [3)]	(2115)	23 Sep - 24 Sep	TS	35
Mindulle [3)]	(2116)	23 Sep - 1 Oct	TY	105

Note: Based on information from the RSMC Tokyo-Typhoon Center.
1) Intensity classification for tropical cyclones.
TS: tropical storm, STS: severe tropical storm, TY: typhoon
2) Estimated maximum 10-minute mean wind.
3) Based on early analysis data, but not best track.

3. Monsoon activity and atmospheric circulation

Convective activity inferred from OLR averaged for June – September 2021 (Figure 3-2) was enhanced from the southeastern tropical Indian Ocean to the Maritime Continent and over the seas south of Japan, and was suppressed over the western and northern tropical Indian Ocean, from the Indochina Peninsula to the seas east of the Philippines and over the seas east of New Guinea, in association with a negative Indian Ocean Dipole (IOD) mode episode, which is characterized by positive SST anomalies in the southeastern tropical Indian Ocean and negative SST anomalies in

the western tropical Indian Ocean, and La Niña-like SST anomalies in the equatorial Pacific (Figure 3-3). OLR index data (Table 3-2) indicate that the overall activity of the Asian summer monsoon (represented by the SAMOI (A) index) was below normal. The active convection area was shifted southward (SAMOI (N) index) and westward (SAMOI (W) index) of its normal position in May, August and September, and northward and eastward from June to July.

Figure 3-4 shows four-month mean 200- and 850-hPa stream function fields for June – September. In the upper troposphere (Figure 3-4 (a)), anti-cyclonic circulation anomalies were seen over southern Eurasia and Eastern Siberia, while cyclonic circulation anomalies were seen over the western tropical North Pacific. In the lower troposphere (Figure 3-4 (b)), cyclonic circulation anomalies straddling the equator were seen over the eastern tropical Indian Ocean, while anti-cyclonic circulation anomalies straddling the equator were seen over the western tropical Pacific. The North Pacific Subtropical High (NPSH) extended southwestward of its climatological extent, and the monsoon trough over Southeast Asia was weaker than normal. Such lower-tropospheric circulation anomalies over tropical Indo-western Pacific Ocean areas were associated with the local convection anomalies described above. In association with the upper-tropospheric ridge over Eastern Siberia, lower-tropospheric anti-cyclonic circulation anomalies were prominent over the area from Eastern Siberia to northern Japan.

In contrast to weaker-than-normal average Asian monsoon activity during summer, convective activity in the region exhibited remarkable intraseasonal fluctuations. Values over India and the Bay of Bengal (Figure 3-5 (a)) were enhanced in the latter half of May, mid-June, mid-August and September, and were suppressed from late June to early July and from the end of July to early August. Convective activity over the Philippines (Figure 3-5 (b)) was enhanced in early June, the latter half of July and early October, and was suppressed in May, mid-August and mid-September. These fluctuations generally corresponded to large-amplitude boreal summer intraseasonal oscillation (BSISO; Lee et al. 2013).

In particular, significant changes in atmospheric conditions were observed from July to August. From the latter half of July to the beginning of August, convective activity was enhanced over the seas south of Japan in association with a stronger-than-normal monsoon trough (not shown). Conditions changed in August, when areas from western to eastern Japan experienced record-heavy rain. A stationary front was strengthened by a significant north-south gradient of temperature in the lower troposphere between the Okhotsk High to the north of Japan and a southward-shifted NPSH expanding to the south of Japan (Figure 3-6 (c)). A continuous confluence of water vapor from continental China and along the margin of the NPSH also contributed to widespread continuous heavy rainfall. The southward shift of the NPSH was related to an overall southward shift of the subtropical jet stream (STJ) over East Asia in the upper troposphere (Figure 3-6 (b)) and suppressed convection over the western tropical North Pacific (Figure 3-6 (a)) in association with phasal transition of the BSISO. The southward shift of the STJ was likely affected by SST anomalies accompanying negative IOD conditions (see also Figure 3-3) and related suppressed convection over the Asian summer monsoon region (Figure 3-6 (a)). A significant southward meandering of the STJ to the west of Japan is considered to have produced favorable conditions for updraft occurrence and persistent rainfall from western to eastern Japan.

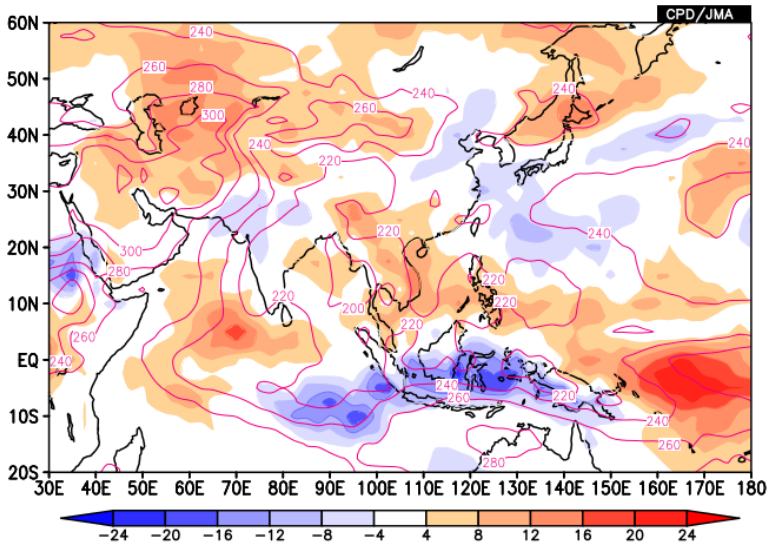

Figure 3-2 Four-month mean OLR [W/m^2] for June–September 2021
Contours indicate OLR at intervals of 20 W/m^2, and color shading denotes OLR anomalies from the normal (i.e., the 1991–2020 average). Negative (cold color) and positive (warm color) OLR anomalies show enhanced and suppressed convection compared to the normal, respectively.

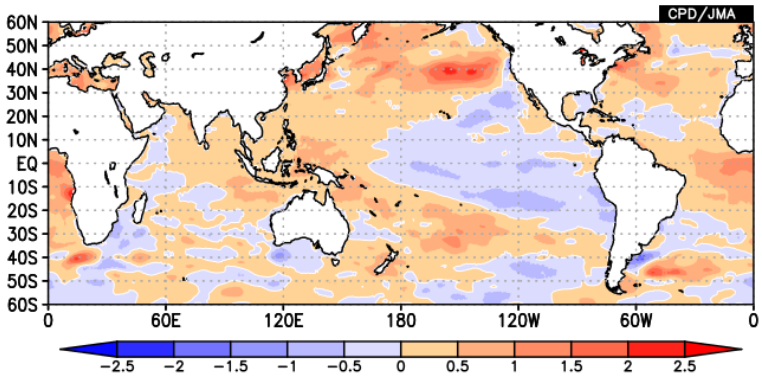

Figure 3-3 Four-month mean SST anomalies [°C] for June–September 2021
The base period for the normal is 1991 – 2020.

Table 3-2 Summer Asian Monsoon OLR Index (SAMOI) values observed from May to September 2021
Asian summer monsoon OLR indices (SAMOI) are derived from OLR anomalies. SAMOI (A), (N) and (W) indicate the overall activity of the Asian summer monsoon, its northward shift and its westward shift, respectively. SAMOI definitions are as follows: SAMOI (A) = (-1) × (W + E); SAMOI (N) = S – N; SAMOI (W) = E – W. W, E, N and S indicate area-averaged OLR anomalies for the respective regions shown in the figure on the right normalized by their standard deviations.

	Summer Asian Monsoon OLR Index (SAMOI)		
	SAMOI (A): Activity	SAMOI (N): Northward-shift	SAMOI (W): Westward-shift
May 2021	-0.7	-2.2	+0.4
Jun 2021	-1.5	+2.1	-0.5
Jul 2021	-0.6	+0.2	-1.8
Aug 2021	-1.6	-0.7	+0.5
Sep 2021	-0.1	-0.2	+0.7

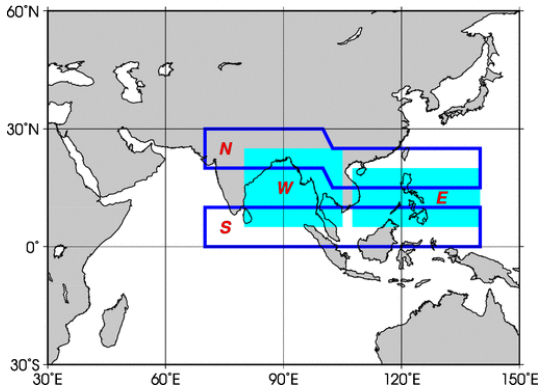

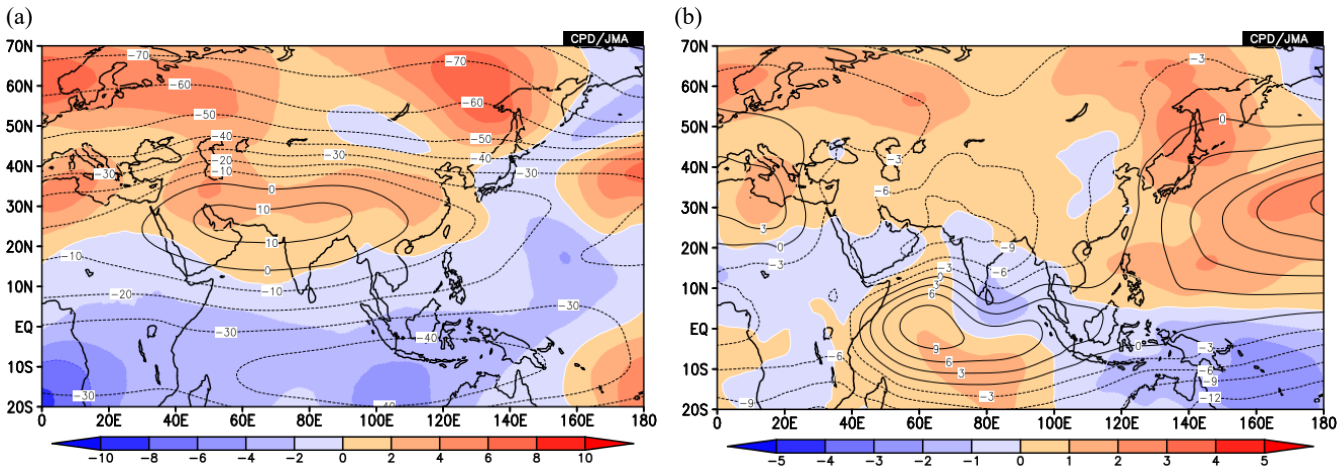

Figure 3-4 Four-month mean (a) 200-hPa and (b) 850-hPa stream function [10^6 m^2/s] for June–September 2021
Contours indicate stream function at intervals of (a) 10×10^6 m^2/s and (b) 3×10^6 m^2/s, and shading shows stream function anomalies. Red (blue) shading denotes anti-cyclonic (cyclonic) circulation anomalies in the Northern Hemisphere, and vice-versa in the Southern Hemisphere. The base period for the normal is 1991 – 2020.

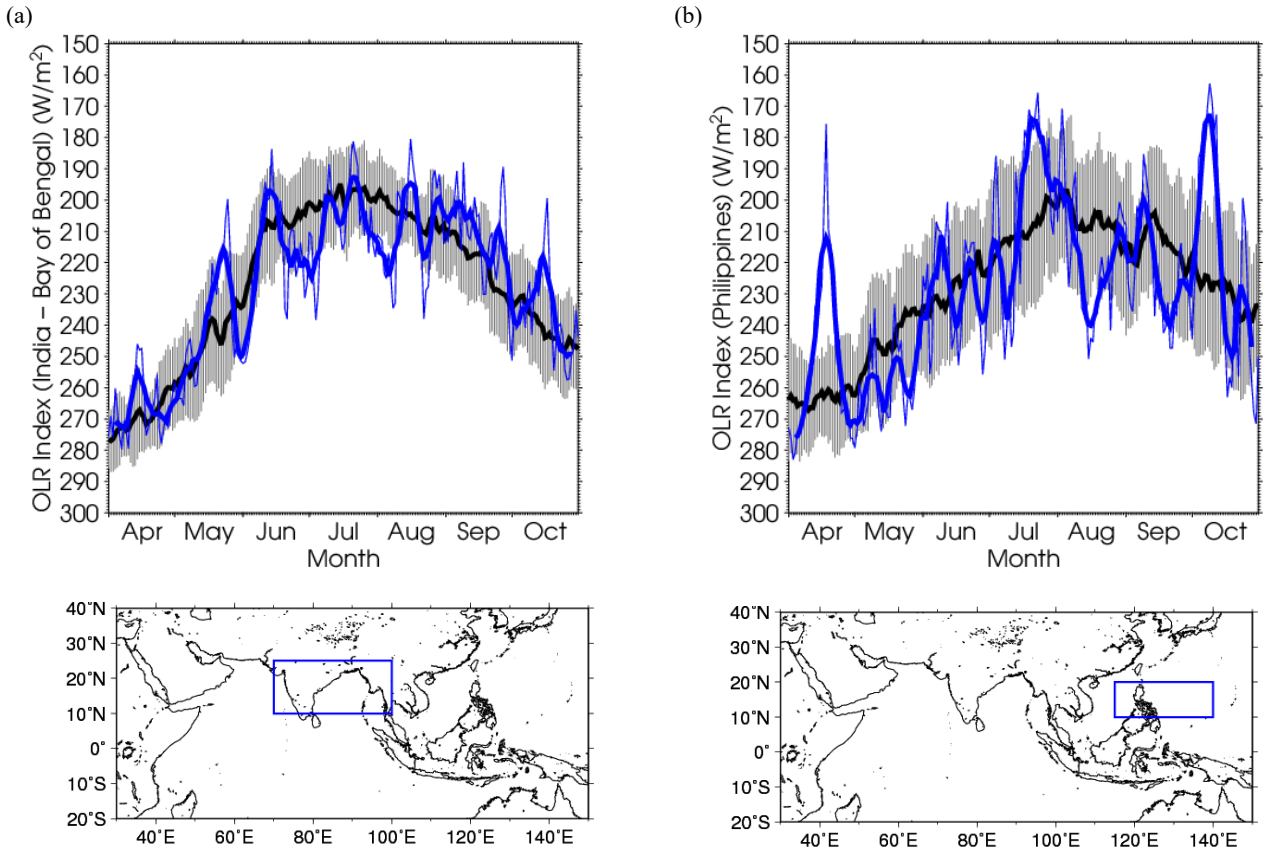

Figure 3-5 Time-series representation of OLR [W/m^2] averaged over (a) India and the Bay of Bengal (shown by the rectangle on the bottom: 10°N - 25°N, 70°E - 100°E) and (b) the Philippines (shown by the rectangle on the bottom: 10°N - 20°N, 115°E - 140°E)
The OLR indices are calculated after Wang and Fan (1999). The thick and thin blue lines indicate seven-day running mean and daily mean values, respectively. The black line denotes the normal (i.e., the 1991 - 2020 average), and the gray shading shows the range of the standard deviation calculated for the time period of the normal.

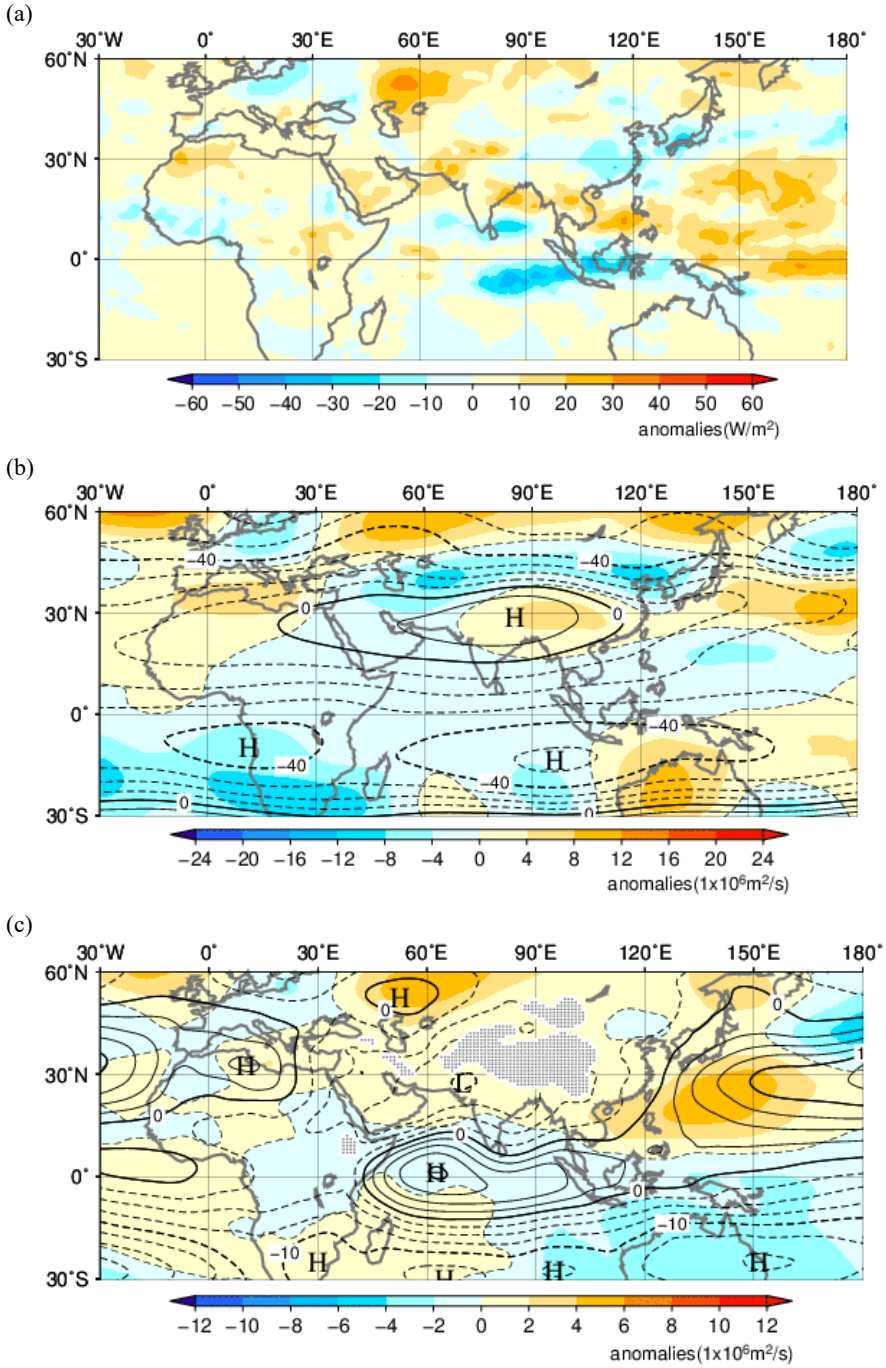

Figure 3-6 Monthly mean (a) OLR anomalies [W/m^2], (b) 200-hPa stream function [10^6 m^2/s] and (c) 850-hPa stream function [10^6 m^2/s] for August 2021

Shading indicates anomalies, and contours show stream function at intervals of (b) 10×10^6 m^2/s and (c) 2.5×10^6 m^2/s. Hatch patterns indicate areas with altitudes exceeding 1,600 m. The base period for the normal is 1991 – 2020.

References

Ishii, M., A. Shouji, S. Sugimoto, and T. Matsumoto, 2005: Objective analyses of sea-surface temperature and marine meteorological variables for the 20th century using ICOADS and the Kobe Collection. *Int. J. Climatol.*, **25**, 865-879.

Kobayashi, S., Y. Ota, Y. Harada, A. Ebita, M. Moriya, H. Onoda, K. Onogi, H. Kamahori, C. Kobayashi, H. Endo, K. Miyaoka,

and K. Takahashi, 2015: The JRA-55 Reanalysis: General specifications and basic characteristics. *J. Meteor. Soc. Japan*, **93**, 5 – 48.

Lee, J.-Y., B. Wang, M. C. Wheeler, X. Fu, D. E. Waliser, and I.-S. Kang, 2013: Real-time multivariate indices for the boreal summer intraseasonal oscillation over the Asian summer monsoon region. *Clim. Dyn.*, **40**, 493-509.

Liebmann, B., and C. A. Smith, 1996: Description of a complete (interpolated) outgoing longwave radiation dataset. *Bull. Amer. Meteor. Soc.*, **77**, 1275–1277.

Wang, B. and Z. Fan, 1999: Choice of South Asian summer monsoon indices. *Bull. Amer. Meteor. Soc.*, **80**, 629–638.

(SATO Hitoshi, Tokyo Climate Center)

<<Table of contents <Top of this article

<<Table of contents